Materials Today Bio 13 (2022) 100195

Contents lists available at ScienceDirect

Materials Today Bio

journal homepage: www.journals.elsevier.com/materials-today-bio

Novel fusion peptides deliver exosomes to modify injectable thermo-sensitive hydrogels for bone regeneration

Shiqing Ma [b], Jinzhe Wu [a], Han Hu [a], Yuzhu Mu [a], Lei Zhang [a], Yifan Zhao [a], Xiaowei Bian [a], Wei Jing [c,d], Pengfei Wei [c,****], Bo Zhao [c,*], Jiayin Deng [a,**], Zihao Liu [a,***]

[a] School and Hospital of Stomatology, Tianjin Medical University, 12 Observatory Road, Tianjin, 300070, China
[b] Department of Stomotology, The Second Hospital of Tianjin Medical University, 23 Pingjiang Road, Hexi District, Tianjin, 300211, China
[c] Beijing Biosis Healing Biological Technology Co., Ltd., No. 6 Plant West, Valley No. 1 Bio-medicine Industry Park, Beijing, 102600, China
[d] Foshan (Southern China) Institute for New Materials, Foshan, 528220, China

ARTICLE INFO

Keywords:
Thermo-sensitive hydrogels
Small intestinal submucosa
Bone regeneration
Exosomes
Mechanical properties
Fusion peptides

ABSTRACT

Injectable thermo-sensitive hydrogels composed of small intestinal submucosa (SIS) with exosomes derived from bone marrow mesenchymal stem cells (BMSCs) are desired for bone regeneration. However, poor mechanical properties limit the clinical application of SIS hydrogels. Herein, the mechanical properties of SIS hydrogels incorporated with 3-(3,4-dihydroxyphenyl) propionic acid (CA) are assessed. The results show that the mechanical properties of SIS hydrogels are improved. In addition, the retention and stability of exosomes over time at the defect site are also challenges. Fusion peptides are designed by connecting collagen-binding domines (CBDs) of collagen type I/III with exosomal capture peptides CP05 (CRHSQMTVTSRL) directly or via rigid linkers (EAAAK). In vitro experiments demonstrate that fusion peptides are contribute to promoting the positive effect of exosomes on osteogenic differentiation of BMSCs. Meanwhile, the results of hydrogels combining exosomes and fusion peptides in the treatment of rat skull defect models reveal that fusion peptides could enhance the retention and stability of exosomes, thereby strengthen the therapeutic effect for skull defects. Therefore, SIS hydrogels with CA modified by fusion peptides and exosomes appear to be a promising strategy in bone regenerative medicine.

1. Introduction

Bone defect is commonly caused by trauma, infection, tumor, congenital diseases and may results in skeletal disorder-derived dysfunction [1,2]. Compared to bone grafting, bone tissue engineering technique has been considered as a potential treatment strategy for bone reconstruction [3,4]. Thermo-sensitive hydrogels that can mimic extracellular matrix (ECM) environment are widely used in bone tissue engineering as scaffold materials [5,6]. They have excellent in situ injectability and morphological adaptability, which are conferred by solution-gel phase transition that occurs with temperature changes [7,8]. Small intestinal submucosa (SIS) is derived from porcine jejunum, composed of nature ECM, including collagen type I, III and various bioactive factors (Table S1, Supporting Information) [9–11]. Collagen molecules in SIS can self-assemble and condense into a three-dimensional (3D) network hydrogel under the influence of temperature (37 °C) [12,13]. Currently, SIS hydrogels are widely used in promoting the regeneration of damaged tissue, because their structure and biological activity can be fine-tuning for desired applications [14,15]. However, under the complex stress condition *in vivo*, due to weak mechanical strength, SIS hydrogels may collapse and impair tissue repair efficacy [16,17]. In order to solve this problem, 3-(3,4-dihydroxyphenyl) propionic acid (CA) with catechol groups is used in hydrogels modification by covalent bonds [18,19]. Catechol groups of CA could interact with collagen molecules in hydrogels and form a cross-linking network between collagen molecules [20], thereby improving mechanical properties of SIS hydrogels.

In addition to beneficial scaffold materials, the osteogenic microenvironment composed of cells, cytokines or other active substances also

* Corresponding author.
** Corresponding author.
*** Corresponding author.
**** Corresponding author.
E-mail addresses: zhaobo@biosishealing.com (B. Zhao), jdeng@tmu.edu.cn (J. Deng), liuzihao@tmu.edu.cn (Z. Liu).

https://doi.org/10.1016/j.mtbio.2021.100195
Received 29 September 2021; Received in revised form 23 December 2021; Accepted 24 December 2021
Available online 27 December 2021

plays an important role for bone regeneration [21]. Bone marrow mesenchymal stem cells (BMSCs) with self-renewal and multiple differentiation potentials have the ability to treat bone injuries [22–24]. However, traditional stem cell transplant may cause low homing efficiency and tumor formation [25,26]. Therefore, it is necessary to find an alternative technology to avoid the limitations of direct cell transplantation. Exosomes, nanovesicles naturally secreted by cells, regulating cell-to-cell communication by transferring mRNAs, miRNAs and proteins between cells [26,27]. The utilization of exosomes-based therapy exhibits an exceptional stability, low immunogenicity and intrinsic homing effect [28,29]. Accumulating studies have confirmed that exosomes derived from BMSCs (BMSCs-Exs) have similar biological effects to BMSCs in inducing osteogenesis [30,31]. Cell-free therapy based on exosomes opens up a new avenue for bone defect repair.

In spite of the advantages mentioned above, the use of exosomes for bone regeneration remains a challenge. At present, a common method of modifying exosomes into hydrogels is direct mixing [32,33], which may have disadvantages such as low loading efficiency, destruction of exosomes structure and hindering the osteogenic potential of exosomes [34]. To overcome these limitations, multifunctional fusion peptides composed of two or more peptide chains, exhibiting excellent capabilities in drug delivery [35–38], are considered as a promising method for exosomes delivery. Pertinent literatures report that CP05 (CRHSQMTVTSRL), a polypeptide sequence, can recognize and capture exosomal marker CD63 specifically [36,39]. TKKTLRT and KELNLVY are collagen-binding domains (CBDs) that bind collagen type I and type III of SIS hydrogels specifically [40–43], respectively. Furthermore, involving a peptide linker in the process of constructing fusion peptides might avoid misfolding or impaired biological activity of fusion peptides [44]. EAAAK is a rigid linker containing α-helix structure that consist of multiple hydrogen bonds, conferring high structural stability to fusion peptides [45,46]. Accordingly, we hypothesize that exosomes could be effectively introduced into SIS hydrogels by constructing fusion peptides linking the CBDs, CP05 and EAAAK together. Herein, we assess the mechanical properties of CA modified SIS hydrogels (SIS-CA). Then investigate the effect of fusion peptides on exosomes in promoting osteogenic differentiation and biological behavior of BMSCs through experiments in vitro. And the osteogenic ability of SIS-CA hydrogels containing exosomes and fusion peptides are evaluated in rat skull defect models. It is expected that this strategy has great application potential in bone regenerative medicine.

2. Materials and methods

2.1. Materials

All fusion peptides were synthesized by Jill Biochemical Co., Ltd. (Shanghai, China). Fresh porcine small intestines were harvested from healthy pigs. The 3-(3,4-two hydroxyphenyl) propionic acid (CA) and the polyvinylidene fluoride (PVDF) membranes were purchased from Sigma-Aldrich (Massachusetts, USA). Dulbecco's modified Eagle's medium (DMEM), fetal bovine serum (FBS), penicillin/streptomycin, type III collagenase were purchased from Gibco (NY, USA). The 1,1-dioctadecyl-3,3,3,3-tetramethylindotricarbocyanine iodide (DiR) and 1,1′-dioctadecyl-3,3,3′,3′-tetramethylindocarbocyanine perchlorate (DiI) were purchased from AAT Bioquest (California, USA). The 4′,6-Diamidino-2-phenylindole, dihydrochloride (DAPI), Live/Dead kit, 4% paraformaldehyde, hematoxylin and eosin (HE) and Masson's trichrome were purchased from Solarbio (Beijing, China). The Cell Counting Kit-8 (CCK-8) were purchased from Synaptic Systems (Goettingen, Germany). Rhodamine B dye were purchased from cytoskeleton Inc. (Denver, USA). The Reverse transcription kit and SYBR Green Master Mix were purchased from Promega (Madison, Wisconsin, USA) and LC480II system were purchased from Roche (Basel, Switzerland). The Ethylenediaminetetraacetic acid slow decalcification solution (EDTA) was purchased from Servicebio (Wuhan, China). The 0.22-m filters were purchased from Millipore (Massachusetts, USA). The Bradford assay and all antibodies were purchased from Abcam (Cambridge Science Park, UK). ExoQuant™ Overall Exosome Capture and Quantification Assay Kit were purchased from Biovision (San Francisco Bay, USA). Sprague Dawley rats (SD, 30 males; 250–280 g) were purchased from the Nankai Experimental Animals Center (Tianjin, China).

Table 1
Fusion peptide sequence.

Fusion peptides	Sequence	Abbreviation
Fusion peptide 1	TKKTLRTCRHSQMTVTSRL	P1 (FITC)
Fusion peptide 2	KELNLVYCRHSQMTVTSRL	P2 (RB)
Fusion peptide 3	TKKTLRTEAAAKCRHSQMTVTSRL	P3 (FITC)
Fusion peptide 4	KELNLVYEAAAKCRHSQMTVTSRL	P4 (RB)

2.2. Design and synthesis of fusion peptides

All fusion peptides sequences were presented in Table 1, using the Fmoc (9-fluorenylmethyloxycarbonyl) method. P1 and P3 labeled with fluorescein isothiocyanate (FITC, green), and P2 and P4 with Rhodamine B (RB, red) markers for confocal laser scanning microscope (CLSM, LSM900; Zeiss, Germany). The structures of the two fusion peptides were predicted and their molecular structures were analyzed by Raptor X v5.1 (Raptor X, USA) software.

2.3. Characterization of BMSC-Exs

Bone marrow mesenchymal stem cells (BMSCs) were inoculated into culture dishes with fresh DMEM, 10% FBS and 1% penicillin/streptomycin, and cultivated in a 5% CO_2 atmosphere at 37 °C. Then, BMSCs medium was collected after the medium was centrifuged at 1000 g for 10 min, followed by 10,000 g for 30 min, the supernatant was collected and filtered with 0.22-m filters. Subsequently, the exosomes were precipitated by ultracentrifugation at 100,000 g for 1 h and the pellet was washed with a lot of PBS, and finally recovered by centrifugation at 100,000 g for 1 h [36]. The total protein concentration of exosomes was quantified by Bradford assay. The morphology of exosomes was detected by transmission electron microscope (TEM, HT7700; HITACHI, Japan). The particle size distribution was measured using Nano Sight (NS300; Malvern, UK). In addition, Western blot analysis was used to identify exosomal markers, and cell extracts were used as control.

2.4. Preparation of SIS-CA hydrogels

The submucosa of the small intestine (SIS) was obtained by mechanically removing the porcine jejunum and washing it in deionized water 3 times [11]. The subsequent procedure involved degreasing (a mixed solution of methanol and chloroform (1:1, v/v) for 12 h), enzyme digestion (0.05% trypsin/0.05% ethylenediaminetetraacetic acid at 37 °C for 12 h), detergent treatment (0.5% sodium dodecyl sulfate (SDS) in 0.9% sodium chloride) and sterilization (0.1% peroxyacetic acid for 30 min). Then, the sample was lyophilized using freeze dryer (GAMMA 2–16 LSC; Christ, Germany), lyophilized SIS was cut into flocculent pieces with a freezer mill (MM400; Retsch, Germany), followed by digested in an aqueous solution consisting of 3% acetic acid and 0.1% pepsin for 48 h to obtain 10% w/v SIS pre-hydrogel. SIS-CA hydrogels were obtained by mixing CA into SIS pre-hydrogel. Briefly, CA was dissolved in distilled water at room temperature, the concentration of CA solution was 0.5 M. Add the CA solution to the pre-hydrogel uniformly, then, adjusted the PH of pre-hydrogel to 7.0 with 2.5 M of NaOH solution and let stand at 37 °C for 30 min.

2.5. Preparation of SIS-CA hydrogels with fusion peptides and BMSC-Exs

The above four fusion peptides were dissolved in deionized water at room temperature to obtain fusion peptide solutions P1-4. Peptide solutions were prepared at the concentration of 200×10^{-6} M. Mixed P1 with P2 and P3 with P4 ($p_{1\&2}$ and $p_{3\&4}$), respectively. 300 μL of 1 μg/μL BMSC-Exs were added into the two solutions (Exs-$p_{1\&2}$ and Exs-$p_{3\&4}$). Subsequently, SIS-CA hydrogels were immersed in Exs-$p_{1\&2}$ or Exs-$p_{3\&4}$ solution at 25 °C for 30 min. Finally, SIS-CA hydrogels with Exs-$p_{1\&2}$ and Exs-$p_{3\&4}$ solution were constructed ($p_{1\&2}$SIS-CA/Exs and $p_{3\&4}$ SIS-CA/Exs).

2.6. Characterization of SIS-CA hydrogels

The microscopy images of SIS and SIS-CA hydrogels were detected by field emission-scanning electron microscopy (SEM, Gemini 300; Zeiss, Germany). Hydrogels were lyophilized at −80 °C for 48 h. The lyophilized samples were coated with a conductive layer of gold scanning electrons. The pore size of hydrogels was analyzed by ImageJ v1.8.0 software. In addition, in order to determine the effects of SIS and SIS-CA hydrogels on cell colonization and infiltration, 2×10^5 BMSCs were uniformly inoculated on the surface of the two hydrogels, and the morphology and distribution of BMSCs were observed by CLSM for 2 and 4 d of culture. Moreover, the chemical element composition of SIS and SIS-CA hydrogels was determined by fourier transform infrared spectrometer (FTIR, Nicolet iS50; Thermo Fisher Scientific, USA) analysis with the transmission mode in the wavenumber wavelength range of 4000–500 cm^{-1}. The mechanical strength of the above two hydrogels was measured under a general condition using a universal testing machine (Instron 5567, USA) equipped with a 0.1 N load cell.

The rheological measurements of hydrogels were carried out by rheometer (AR-G2; TA Instrument, USA) with 20 mm cone plate. 1) Under the constant temperature of 37 °C, the storage modulus (G') of SIS and SIS-CA hydrogels were monitored with a frequency of 1hz and a stress-strain of 1% over time. 2) At a fixed angular frequency (10 rad s^{-1}), measured the G′ and loss modulus (G″) of the hydrogels under the strain amplitude sweep (γ = 0.1%–1000%).

The degradation of SIS and SIS-CA hydrogels were studied in degradation solutions composed of PBS and 100 U/mL type III collagenase. The 1 mL hydrogels equal weight, immersed in 10 mL of degradation solution at 37 °C. The hydrogels were collected continuously within 10 d. The weights of lyophilized hydrogels after degradation were defined as W_t. The initial weights of lyophilized hydrogels were recorded as W_0. The degradation rates were calculated according to the following formula:

$$Degradation\ (\%) = (W0 - Wt)/\ W0 \times 100\% \quad (1)$$

2.7. Characterization of p1&2SIS-CA/Exs and p3&4 SIS-CA/Exs hydrogels

The surface morphology of SIS-CA, SIS-CA/Exs, $p_{1\&2}$SIS-CA/Exs and $p_{3\&4}$ SIS-CA/Exs hydrogels was evaluated using SEM. The samples were lyophilized at −80 °C for 48 h. The samples were coated with a gold scanning electron conductive layer. Moreover, to investigate exosomes and fusion peptides were loaded on SIS-CA hydrogels, exosomes were labeled with DiR. In a nutshell, mixed 1 μL of DiR dye solution with DMSO as stock solution. The stock solution was diluted with PBS to 5 mM working solution. the exosomes were mixed with 20 μL working solution. Next, mixed the 200×10^{-6} M $p_{1\&2}$ and $p_{3\&4}$ solutions with the exosomes (DiR) solution, respectively. The SIS-CA hydrogels were divided into three groups. Hydrogels immersed in exosomes (DiR) solusion after lyophilized named SIS-CA/Exs were considered as control, while immersed in Exs (DiR)-$p_{1\&2}$ or Exs(DiR)-$p_{3\&4}$ were named $p_{1\&2}$SIS-CA/Exs or $p_{3\&4}$SIS-CA/Exs. The samples were washed three times with PBS. Images were captured using a CLSM.

2.8. Turbidity test

The effect of CA and fusion peptides on thermo-sensitive properties of hydrogels was investigated by turbidity test. The absorbance of different hydrogels (SIS, SIS-CA, $p_{1\&2}$SIS-CA, $p_{3\&4}$SIS-CA) at different temperatures was measured by UV–Vis spectrophotometer (U-3900, HITACHI, Japan) at 350 nm wavelengths. The heating rate is 2 °C/3min, and the heating range is 20 °C–45 °C.

2.9. Stability test of hydrogels

First, the stability of SIS-CA/Exs, $p_{1\&2}$SIS-CA/Exs and $p_{3\&4}$SIS-CA/Exs hydrogels in collagenase solution was determined by detecting the amounts of exosomes released. Exosome release was tested by Exo-Quant™ Overall Exosome Capture and Quantification Assay Kit. Briefly, 300 μL of 1 μg/μL exosomes solution were used to prepare hydrogels. Then, these hydrogels were placed in collagenase solution at 37 °C. The supernatant was continuously collected for 8 d, and the cumulative release of exosomes was calculated. Then, CLSM was used to further verify the stability of $p_{1\&2}$SIS-CA/Exs and $p_{3\&4}$SIS-CA/Exs hydrogels under inflammatory conditions. BMSCs were inoculated in 6-well plates, TNF-α (10 ng/mL) and IFN-γ (10 ng/mL) were added to the medium to simulate inflammation environment, and BMSC medium was collected. The hydrogels containing fluorescently labeled exosomes and peptides ($p_{1\&2}$SIS-CA/Exs and $p_{3\&4}$SIS-CA/Exs) were placed in the collected medium, and the fluorescence intensity of exosomes and peptides in the hydrogels was observed by CLSM after 1, 5, and 10 days.

2.10. Exosomes uptake assay

After the above hydrogels were dialyzed in distilled water for 3 d and sterilized under 365 nm ultraviolet light for 30 min, they were injected into 12-well plates, and then 2×10^4 BMSCs were seeded on each well. The cells were fixed and stained with DAPI for 10 min. Exosomes were labeled with DiI. The results were observed by the CLSM after incubated 1 d.

2.11. Cell viability, proliferation and adhesion

After incubated with hydrogel extracts (SIS-CA, SIS-CA/Exs, $p_{1\&2}$SIS-CA/Exs, $p_{3\&4}$SIS-CA/Exs, Blank as the control group) for 1, 2and 3 d, the cells were stained with Live/Dead kit for 5min to test cell viability. Images were obtained using a fluorescence microscope.

CCK-8 was used to evaluate the proliferation of the BMSCs in different groups. During 6 d of culture, the cells were incubated with counting reagents for 3 h every day. The relative cell number was determined by measuring the absorbance (OD) at 450 nm with a microplate reader (Multiskan FC, Thermo Fisher Scientific, USA).

To observe the cytoskeleton and adhesion of cells in different groups, cells were fixed in 4% paraformaldehyde solution for 15 min and permeated in 0.5% Triton X-100 for 10 min after incubated for 12 and 24 h. Actin was stained with Rhodamine B to show the cytoskeleton. DAPI was used to stain the nucleus. Cell morphology was observed by CLSM.

2.12. Real-time quantitative polymerase chain Reaction(qRT-PCR)

To reveal the potential mechanism of hydrogels effect on the differentiation of BMSCs, qRT-PCR analysis was carried out in each group. After the cells were cultured in osteoinduction medium or basal medium (without osteoinduction conditions) for 14 days, total RNA was extracted

with TRIzol. Reverse transcription kit to synthesize cDNA. SYBR Green Master Mix and LC480II system were used for analysis. The sequences of primers are listed in Table S2(Supporting Information). Results were normalized to GAPDH.

2.13. Western blot analysis

The proteins of BMSCs cultured for 14 d were separated by gel electrophoresis and transferred to PVDF membranes. PVDF membranes were submerged in the primary antibodies (1:1000 dilution for 12 h at 4 °C). Membranes were then incubated with a secondary antibody (1:5000 dilution for 1 h at 25 °C). The antibody-bound proteins were detected using a Pierce ECL Western Blotting Substrate (Thermo Fisher Scientific, USA). The quantitative analysis was quantified using ImageJ software v1.53.

2.14. Immunofluorescence staining

Inoculated 1×10^4 BMSCs in a 24-well plate and incubated with 1 mL of SIS-CA, SIS-CA/Exs, $p_{1\&2}$SIS-CA/Exs, $p_{3\&4}$SIS-CA/Exs hydrogel extracts, with or without osteoinduction, Blank as control. Afterwards, the BMSCs were fixed with 4% paraformaldehyde for 30 min, permeabilized with 0.5% Triton X-100 for 10 min, and blocked with 5 mg/mL BSA solution for 1 h. Then, incubate the cells with the primary antibody (1:200 dilution for 12 h at 4 °C). Afterwards, they were incubated with Cy3 conjugated secondary antibody (1:1000 dilution for 1 h at 25 °C), and then stained with 1 mg/mL DAPI for 10 min. CLSM was used to observe fluorescence images.

2.15. Animal experiment

All procedures were approved by the Animal Ethics Committee of Tianjin Medical University of Science and Technology. SD Rats were anesthetized by isofrane inhalation. Surgery was performed under aseptic conditions. A circular 8 mm hole (made by a high-speed drill with an 8 mm round hole opener) in the dorsal side of the skull was used to observe the ability of hydrogels to promote bone regeneration *in vivo*. Animals were randomly divided into five groups: 1) Blank (n = 6), 2) SIS-CA (n = 6), 3) SIS-CA/Exs (n = 6), 4) $p_{1\&2}$SIS-CA/Exs (n = 6) and 5) $p_{3\&4}$SIS-CA/Exs (n = 6). During the initial operation, hydrogels immersed in different mixture were implanted into the defect sites. Subsequently, hydrogels containing different components were injected into the defects once a week. Specifically, 10% w/v SIS-CA pre-hydrogel was mixed with NaOH solution to obtain neutral SIS-CA hydrogel solution and stored at 4 °C. Then, the hydrogel solution was blended with the peptide-exosomal solution or pure exosomal solution according to the above method, the mixture was loaded into a 5 mL syringe. The needle penetrated the skin tissue at the top of the defect and injected the mixture into the defect site.

2.16. Micro-CT analysis of bone defects

A micro-CT scanner (SkyScan 1276; Bruker, Germany) was applied to evaluate the regeneration of the defect on the cranium. Rats were euthanasia 12 weeks after operation, skulls were explanted and fixed in 4% paraformaldehyde. Three-dimensional construction of each specimen was observed with CTvox v3.3 software. The CT-analyzer v1.17 software was used to analyze bone volume/tissue volume (BV/TV) of each group.

2.17. Histological and immunohistochemical staining

Specimens were decalcified in EDTA at room temperature for 1mths. The specimens were embedded in paraffin and cut into 5 mm thick sections. Subsequently, the sections were stained with hematoxylin and eosin (HE) and Masson's trichrome (Solarbio, China) for histological analysis.

Immunohistochemical (IHC) staining for RUNX2 was conducted. The primary antibodies with fluorescence-conjugated secondary antibody IgG (1:200 dilution). The stained sections were photographed with Vectra Polaris (PerkinElmer, USA). Subsequently, images were visualized by NDP. view 2 Inc software.

2.18. Statistical analysis

All data were presented as the mean ± standard deviation (SD). Statistical analysis was performed using SPSS v22.0 software. Statistical significance was tested by one- or two-way ANOVA to determine significant statistical differences between data. P-value is less than 0.05(*$p < 0.05$), 0.01(**$p < 0.01$), 0.001(***$p < 0.001$) were considered indicative of statistical significance.

3. Results and discussion

3.1. Structure Prediction of fusion peptides

The predicted pseudo-3D architectures of the four fusion peptides are shown in Fig. 1. The fusion peptides P1 and P2 were composed of 2 parts, CP05 and collagen-binding peptide I/III, while P3 and P4 consisted of 3 parts, CP05, collagen-binding peptide I/III, and a peptide linker EAAAK. In this study, EAAAK was selected as a linker to construct ideal fusion peptides. EAAAK is a rigid linker containing a lot of hydrogen bonds, which can maintain a reasonable distance between the functional domains of fusion proteins, reduce mutual interference between the linked parts, and make fusion peptides have higher structural stability [47]. In the case of fusion peptides with EAAAK, the number of hydrogen bonds (red line segments between helical frames) in P3 and P4 was much more than P1 and P2, exhibiting compact skeleton structure. This may be beneficial for CP05 to capture more exosomes and efficiently anchor the exosomes to SIS hydrogels through CBDs.

3.2. Preparation and characterization of SIS-CA hydrogels

SIS in pepsin-acetic acid mixed solution formed transparent acid pre-hydrogel solution at a concentration of 10% (w/v). Take part of the solution to add CA. After the pH was adjusted to 7.0 and incubated at 37 °C for 1 h, SIS and SIS-CA hydrogels were observed (Fig. 2). CA grafted SIS hydrogels to improve mechanical properties of the hydrogels as shown in Fig. 2. SIS was firstly self-assembled into a 3D network at 37 °C in a neutral environment by formation of amide bonds (–CO–NH-, N-terminal in collagen molecules reacted with C-terminal). Subsequently, catechol groups of CA were grafted on collagen molecules by reacting with -NH2. When catechol groups were oxidized to quinone, they reacted with unoxidized catechol to establish a linking bridge among collagens and enhance crosslinking of hydrogels [48]. In particular, the UV–Vis spectrophotometer explored the effect of CA on thermo-sensitive properties of hydrogels. Hydrogels were liquid at relatively low temperature, with low refractive index and low turbidity. As the temperature rises, the hydrogel network was integrated, and water was drained from it, resulting in a change in absorbance. The temperature at which the absorbance changes suddenly was the gelation temperature (Tt) of hydrogels. The results (Fig. S2a) show that the Tt of SIS hydrogels was about 37 °C, and that of SIS-CA hydrogels was 27.5 °C, because the crosslinking degree of hydrogels was increased and the dehydration speed was accelerated and the gelation time became shorter after CA addition [49].

The morphologies and chemical compositions of SIS-CA hydrogels

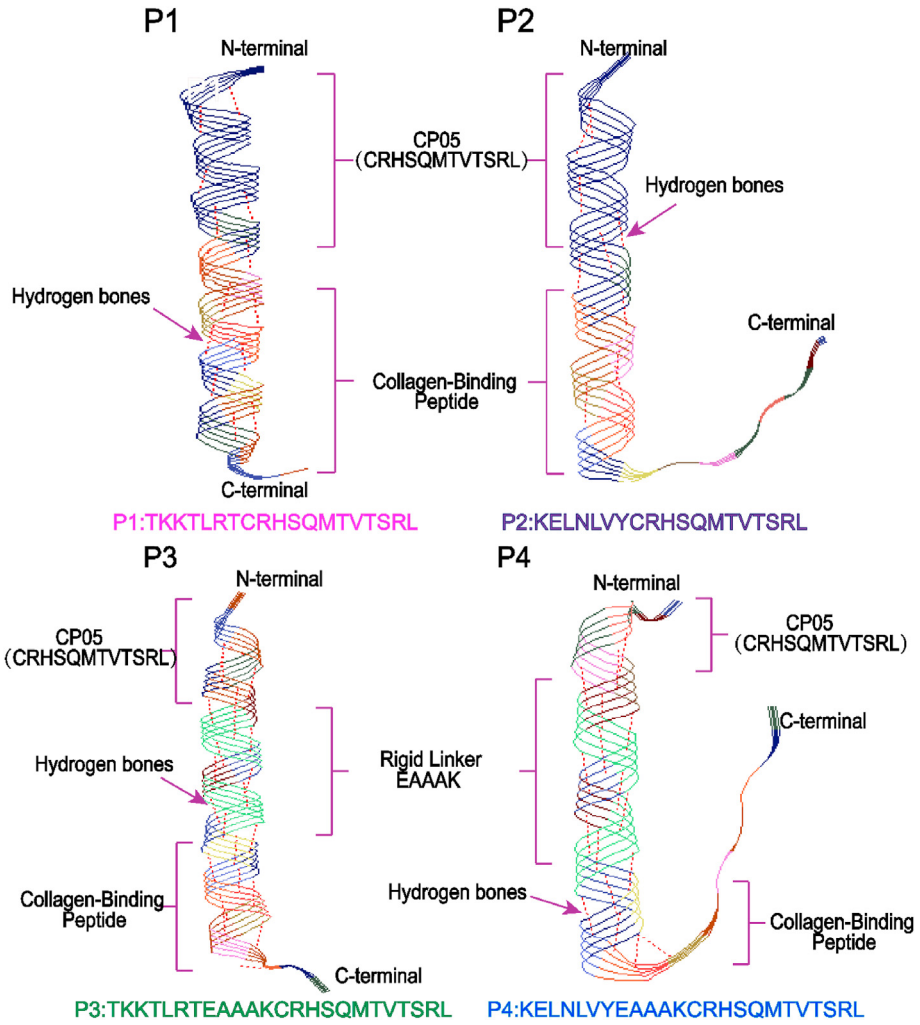

Fig. 1. Pseudo-3D views of molecular architectures. The structures of fusion peptides P1, P2, P3 and P4 were predicted by Raptor X. The N- and C-termini were labeled.

were characterized by scanning electron microscope (SEM) and fourier transform infrared spectroscopy (FTIR). The interconnected 3D porous microstructure of the two hydrogels was illustrated in Fig. 3a. Pristine SIS hydrogels contained large pores. On the contrary, hydrogels became more compact as CA added, which the tertiary structure was integrated. Pore size analysis results show that the pore size of the SIS hydrogel was 118.40 ± 38.41 μm, while that of SIS-CA was 70.52 ± 16.10 μm (Fig. 3b). In order to explore whether the reduction of the pore size of hydrogels has an effect on BMSCs colonization and infiltration, this study used confocal laser scanning microscope (CLSM) to observe the distribution of cells in the two hydrogels for 2 and 4 days. The 3D image (Fig. S1) showed that the morphology of BMSCs was not significantly different. Depth analysis showed that the infiltration degree of the cells in the two hydrogels was both 12 μm for 2 d, and 20 μm for 4 d. Obviously, there was no significant difference in the infiltration rate. This result demonstrated that after adding CA, although the pore size of hydrogels was reduced, it had no obvious positive or negative effect on the colonization and infiltration of BMSCs. Next, FTIR spectra (Fig. 3c) shows that the adsorption bands at 1636 cm^{-1} and 1542 cm^{-1} were associated with vibration of amide I (C═O) and stretching vibration of amide II (C–O) from collagens, these are characteristic peaks of SIS hydrogels [50]. The changes of characteristic peak position represent the change of substance molecular configuration [51]. After CA modification, amide I band just shifted 1 cm^{-1} to higher wavenumber while amide II had no shift, suggesting that collagen structure was not altered. In addition, decreased transmittance of amide I and II implied that their content increased in SIS hydrogels, indicating CA was effectively grafted into SIS hydrogels.

Favorable mechanical properties are indispensable for bone tissue engineering scaffold materials, to investigate the influence of CA on the tensile property of SIS hydrogels, load-displacement curves were measured. The results show improved mechanical properties of SIS hydrogels, with the maximum load of 2.8 ± 0.12 N. Specifically, the maximum load of SIS-CA hydrogels was almost 3-fold higher than that of SIS hydrogels (Fig. 3d). This mechanical reinforcement may be attributed to quinone, which is oxidized from catechol bases, cross-links with collagens to form tough hydrogels. In order to gain insight into the mechanical properties of SIS hydrogels, the rheological characteristics of SIS and SIS-CA hydrogels were determined using a cone plate rheometer. It was found that the mechanical strength of SIS-CA hydrogels was higher than SIS hydrogels. The maximum storage modulus(G′) of SIS hydrogels was 21.36 ± 0.25 Pa, while it increased 1.4-fold with CA (Fig. 3e). Moreover, the G′ and the loss modulus(G″) intersecting curves of SIS and

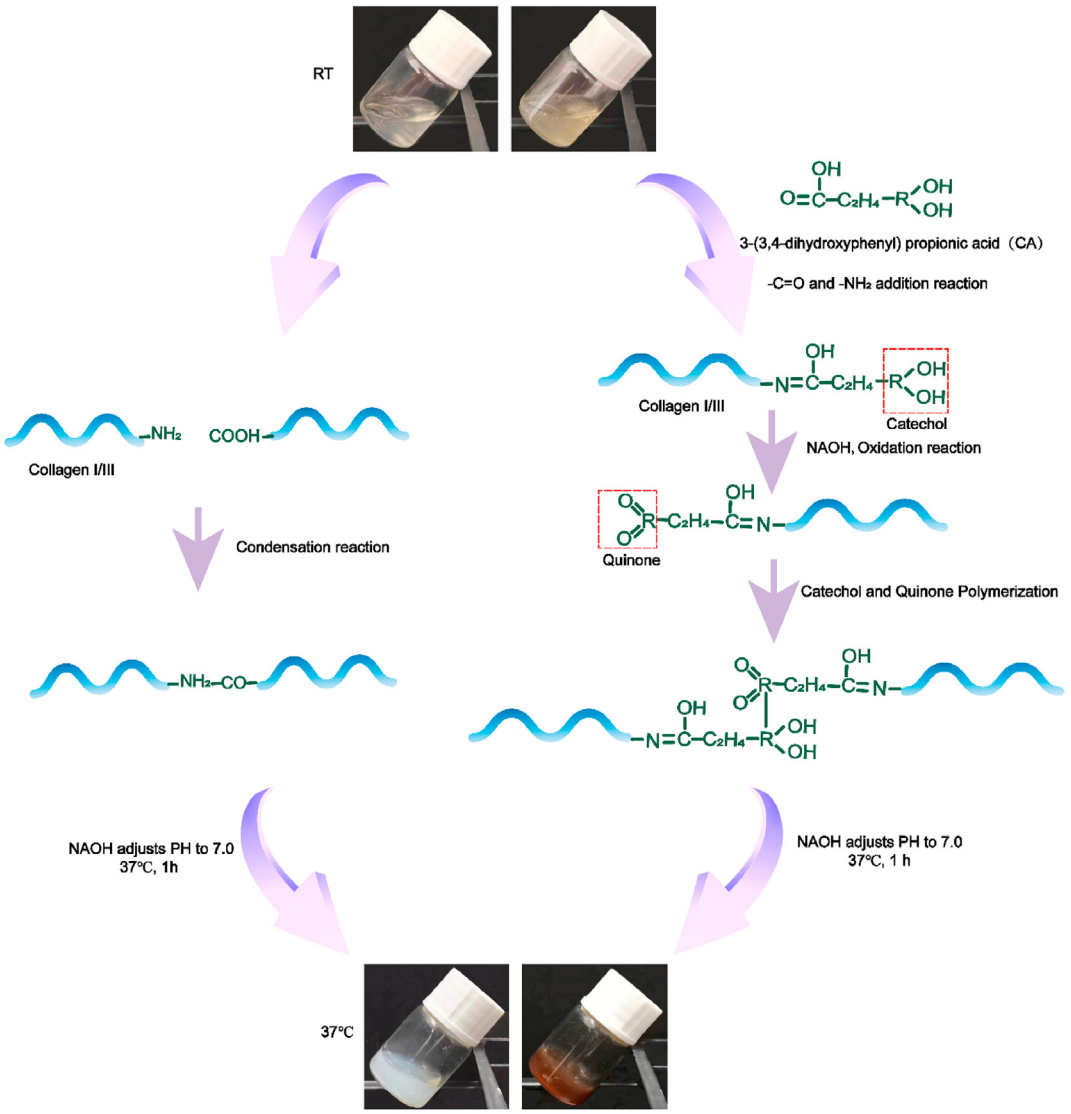

Fig. 2. Schematic illustration of the construction process of SIS hydrogels and SIS-CA hydrogels.

SIS-CA hydrogels representing the critical point of hydrogels collapse appeared at approximately 205% and 275% strain, respectively (Fig. 3f and g). In addition, the degradation studies of two hydrogels were carried out in type III collagenase solution (100 U/mL) at 37 °C within 10 d. The results in Fig. 3h show that the degradation rate of SIS-CA hydrogels is lower than the other one (the final degradation rates are 70.9% and 92.4%, respectively). The conclusion that CA is useful for improving the mechanical properties of hydrogels is confirmed.

3.3. Synthesis and characterization of SIS-CA hydrogels with fusion peptides and BMSC-Exs

BMSCs-Exs were extracted by differential centrifugation. Transmission electron microscopy (TEM), Nano Sight and Western blot were performed to identify BMSCs-Exs. The results show a classical cup-shaped morphology (Fig. 4a) of BMSCs-Exs, with a diameter of 122 nm (Fig. 4b), which is in line with the general diameter range [52,53]. Western blot analysis revealed that Alix, CD9 and CD63, which are specific surface markers of exosomes, were present in exosomes, while Cytochrome C, a specific marker of cytosolic, was only present in cells (Fig. 4c) [54]. Subsequently, BMSCs-Exs was incorporated into SIS-CA pre-hydrogel solution directly or via fusion peptides, thereby obtaining SIS-CA/Exs, $p_{1\&2}$SIS-CA/Exs and $p_{3\&4}$SIS-CA/Exs hydrogels.

The microstructure of SIS-CA hydrogels was altered by fusion peptides. As shown in Fig. 4d, f and g, pristine SIS-CA hydrogels displayed fiber cross-linked pores, and the 3D pores of $p_{1\&2}$SIS-CA/Exs and $p_{3\&4}$SIS-CA/Exs hydrogels were filled with tiny fusion peptide crystalline particles (white arrows). However, no exosomes were observed in the SEM images (Fig. 4e). In order to further demonstrate whether the BMSCs-Exs and fusion peptides were modified on SIS-CA hydrogels, CLSM verified the loading of exosomes and fusion peptides (Fig. 4h). After rinsing three times with PBS, only faint purple fluorescence of BMSCs-Exs (DiR labeled) was present in SIS-CA/Exs hydrogels without any fusion peptides. In contrast, high density purple fluorescence, green fluorescence (Fluorescein isothiocyanate, FITC-labeled type I collagen fusion peptides), and red fluorescence (Rhodamine B, RB-labeled type III collagen fusion peptides) appeared in the images of $p_{1\&2}$SIS-CA/Exs and $p_{3\&4}$SIS-CA/Exs hydrogels, indicating exosomes were efficiently

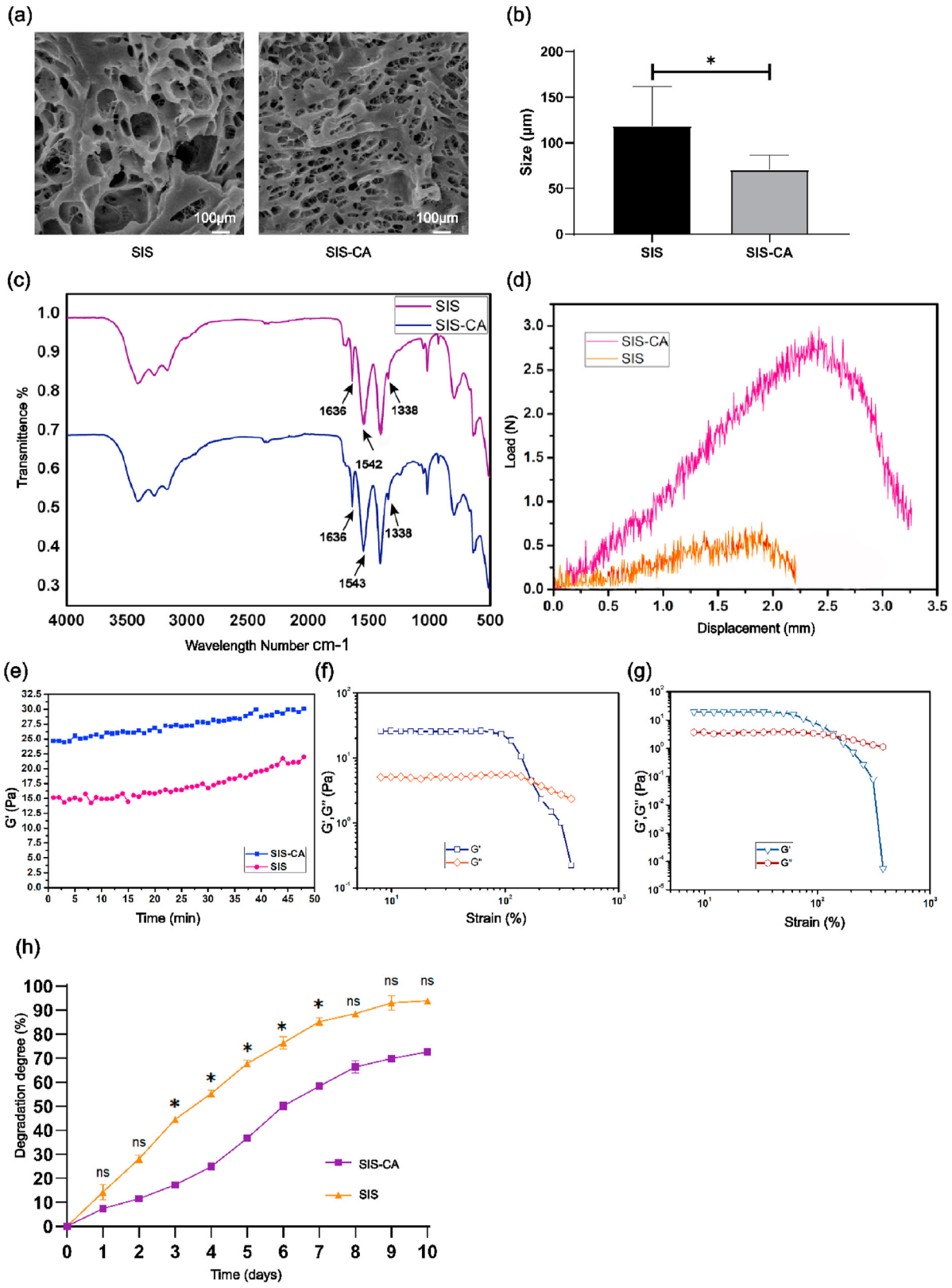

Fig. 3. Characterization of hydrogels. (a) SEM images of SIS and SIS-CA hydrogels. (b) Pore size of SIS and SIS-CA hydrogels (c) FTIR spectra of the SIS and SIS-CA hydrogels. (d) Tensile load-displacement curves of SIS and SIS-CA hydrogels. Rheological behavior of SIS and SIS-CA hydrogels. (e) Representative curves of the gelation kinetics of the SIS and SIS-CA hydrogels were determined by monitoring changes in the storage modulus(G′) after inducing gelation. The G′ and loss modulus(G″) of the (f) SIS, (g) SIS-CA hydrogels from strain amplitude sweep ($\gamma = 0.1\%–1000\%$) at a fixed angular frequency (10 rad s^{-1}). (h) Degradation rate of SIS and SIS-CA hydrogels in type III collagenase solution within 10 d *$p < 0.05$.

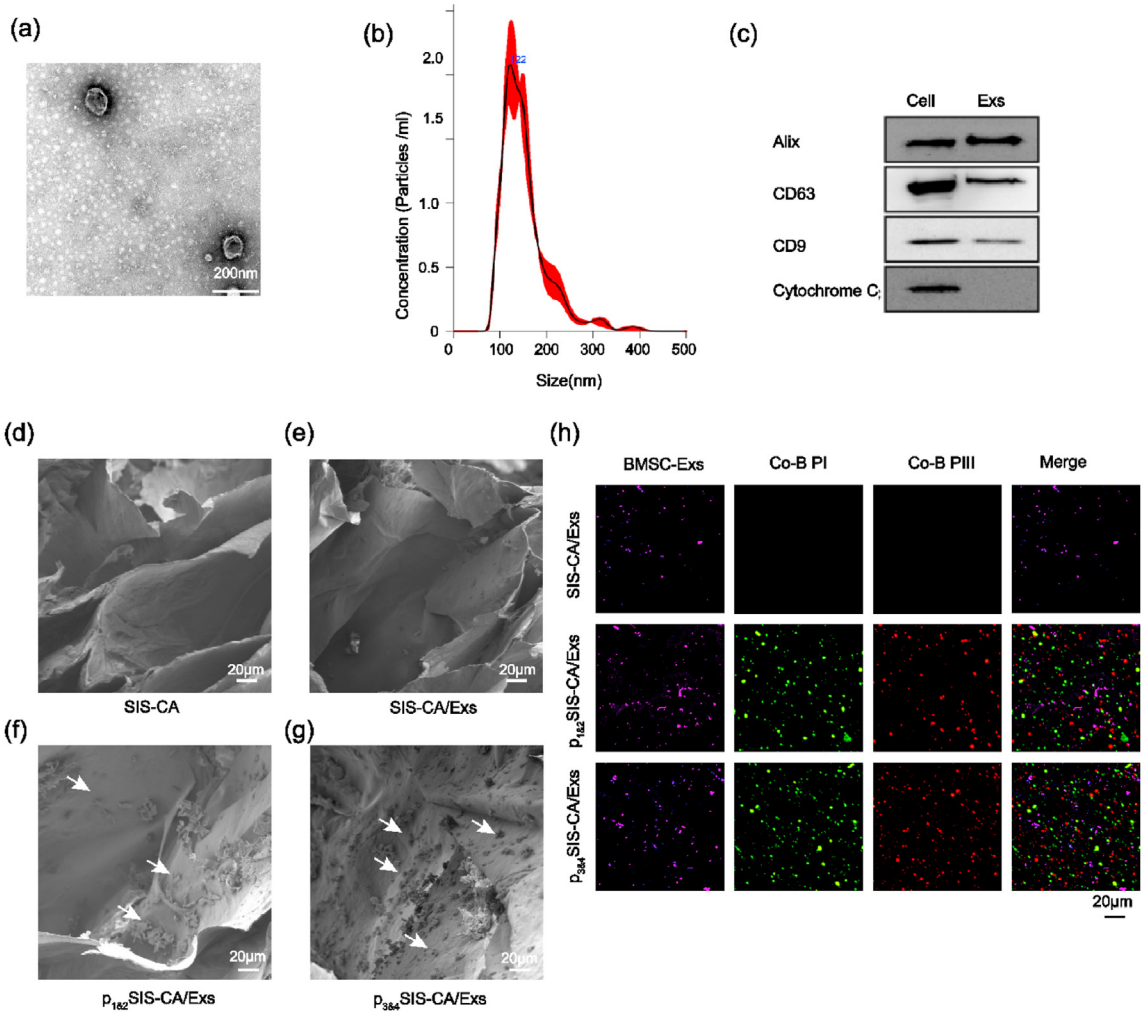

Fig. 4. Identification of exosomes and characterization of exosomes and fusion peptides loaded on hydrogels. (a) Morphology of BMSCs-Exs observed by TEM. (b) Particle size distribution of BMSCs-Exs detected by NanoSight. (c) Western blot analysis of exosomal and the cell nuclei surface markers, Alix, CD63, CD9 and Cytochrome C. SEM images of (d) SIS-CA, (e) SIS-CA/Exs, (f) $p_{1\&2}$SIS-CA/Exs, (g) $p_{3\&4}$SIS-CA/Exs hydrogels. (h) Observation of the load of BMSCs-Exs and fusion peptides on SIS-CA, SIS-CA/Exs, $p_{1\&2}$SIS-CA/Exs, $p_{3\&4}$SIS-CA/Exs hydrogels with CLSM. White arrows: fusion peptides, Co–B PI: collagen-binding peptide I, Co–B PIII: collagen-binding peptide III.

anchored to hydrogels by fusion peptides. Particularly, compared with $p_{1\&2}$SIS-CA/Exs hydrogels, the fluorescence of BMSCs-Exs and fusion peptides on $p_{3\&4}$SIS-CA/Exs hydrogels were slightly stronger and more uniform distribution, which may be related to the contribution of EAAAK. The existence of EAAAK could make CP05 and CBDs of fusion proteins have a fixed distance in space, so that they do not interfere with each other, more fusion peptides with a large number of exosomes bound to hydrogels. Furthermore, turbidity analysis showed that there was almost no change in Tt after mixing the fusion peptides into hydrogels, that is, the thermo-sensitive properties of hydrogels did not change (Fig. S2b).

3.4. SIS-CA/Exs hydrogels with fusion peptides stimulating the proliferation and adhesion of BMSCs in vitro

Stable and sustained release of exosomes is essential to promote proliferation and osteogenic differentiation of cells. Fig. 5a shows the release curves of different hydrogels in the collagenase solution. The $p_{3\&4}$SIS-CA/Exs hydrogels had relatively low release rate compared with the other two hydrogels. After continuous measurement for 8 d, the final concentration of exosomes detected in the $p_{3\&4}$SIS-CA/Exs hydrogel extract was 54.11 ± 2.03%, while it in the $p_{1\&2}$SIS-CA/Exs hydrogels extract was 50.41 ± 1.23%. On the contrary, the release of exosomes from SIS-CA hydrogels stopped on the 6th d, and the cumulative release of exosomes was the least. This is not only because the hydrogels initially captured the least of exosomes, but also the hydrogels lacked the fusion peptides and did not have the effect of sustained release of exosomes. In order to further explore the stability of the materials, $p_{1\&2}$SIS-CA/Exs $p_{3\&4}$SIS-CA/Exs hydrogels were placed under inflammatory conditions to observe the degradation of exosomes and fusion peptides at 1, 5 and 10 d. Images show that even under the stimulation of inflammatory factors (TNF-α and IFN-γ), BMSCs-Exs and fusion peptides could still be degraded steadily and continuously from hydrogels (Fig. S3), which confirms the stability of SIS-CA hydrogels from another point of view. Moreover, to prove that exosomes can be taken up by cells and have an effect on cell number, BMSCs was incubated on different hydrogel surfaces. Upright fluorescence microscope analysis of BMSCs-Exs uptake after 1 d culture. As shown in Fig. 5b, BMSCs-Exs (red color, DiI-labeled)

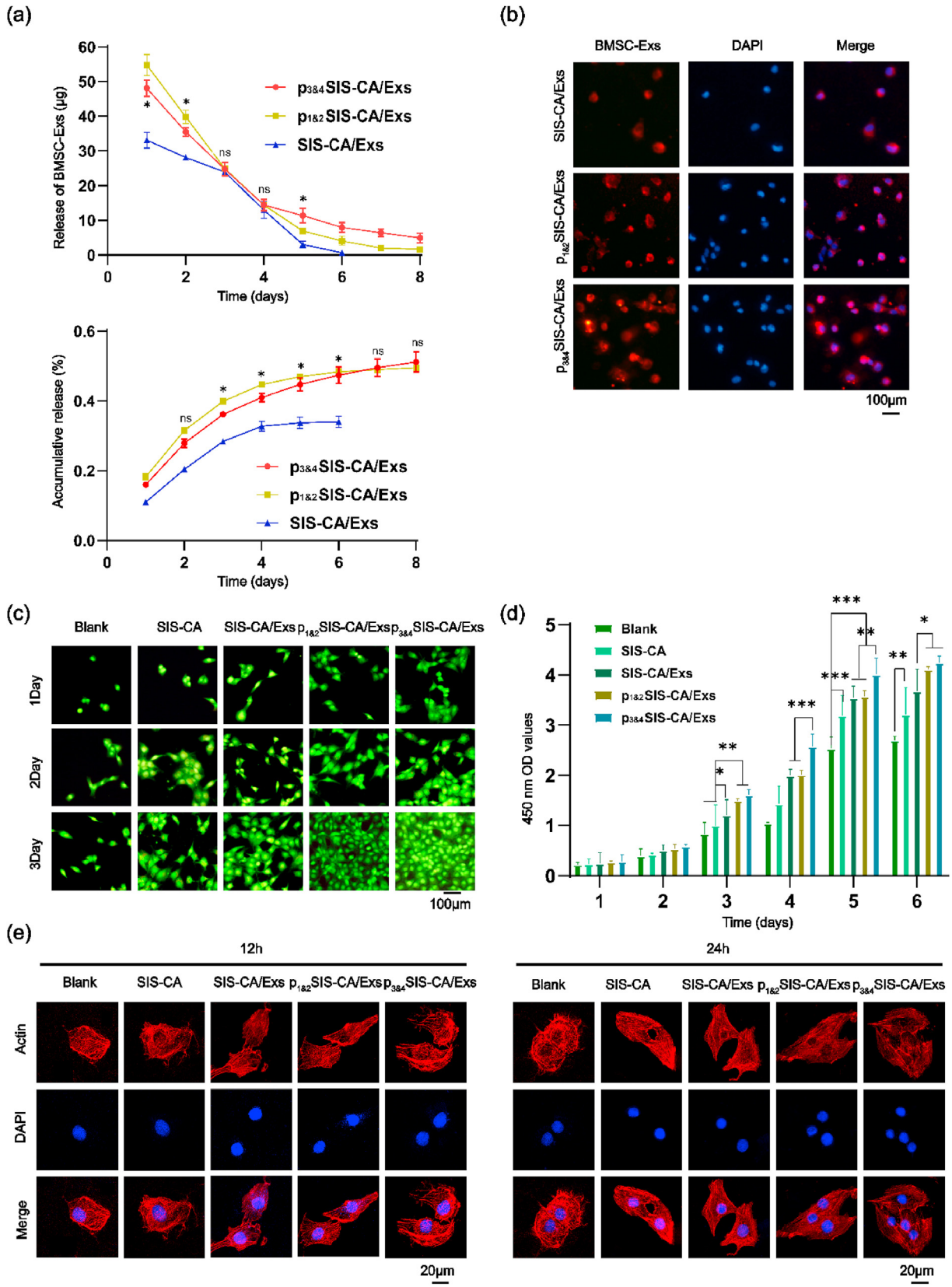

Fig. 5. Effects of exosomes and fusion peptides on BMSCs proliferation and adhesion behavior. (a) exosomes release from SIS-CA/Exs, $p_{1\&2}$SIS-CA/Exs and $p_{3\&4}$SIS-CA/Exs hydrogels in collagenase solution. (b) The diagram of BMSCs-Exs uptaked by BMSCs on SIS-CA/Exs, $p_{1\&2}$SIS-CA/Exs and $p_{3\&4}$SIS-CA/Exs hydrogels for 1 d in vitro. The nuclei of BMSCs were stained with DAPI (blue). (c) Cell Live/Dead staining at 1, 2 and 3 d of culture in pure plastic plates, SIS-CA, SIS-CA/Exs, $p_{1\&2}$SIS-CA/Exs and $p_{3\&4}$SIS-CA/Exs hydrogel extracts, viable cells(green) and dead cells(red). (d) CCK-8 analyzed the effects of SIS-CA, SIS-CA/Exs, $p_{1\&2}$SIS-CA/Exs and $p_{3\&4}$SIS-CA/Exs hydrogels on the proliferation of BMSCs within 6 d (n = 6). (e) Observation of cell adhesion during 12 and 24 h incubation with different hydrogel extracts. DAPI(Blue) labeled nucleus. *$p < 0.05$, **$p < 0.01$ and ***$p < 0.001$.

could be taken by BMSCs and distributed around the nucleus. The results of cells on $p_{3\&4}$SIS-CA/Exs hydrogels absorbed the most exosomes highlight the role of fusion peptides with EAAAK.

Live/Dead assay was employed to characterize the biocompatibility of hydrogels to BMSCs. The image (Fig. 5c) shows that almost no dead cells existed (green cytoplasm without red nuclei) in all groups, and the green fluorescence increased gradually with incubation time prolonging. Moreover, the cells number of $p_{3\&4}$SIS-CA/Exs hydrogels was always larger than that of other hydrogels, indicating $p_{3\&4}$SIS-CA/Exs hydrogels have a stronger effect on promoting cell survival and proliferation. This is probably because hydrogels contained P3 and P4 fusion peptides provided more BMSCs-Exs where miRNA is a key factor stimulating the proliferation and activity of BMSCs. Additionally, CCK-8 assay was performed to further evaluate cell proliferation over 6 d. The graph (Fig. 5d) shows that in all groups, the number of cells showed an upward trend. On the 6th d, the number of cells of the SIS-CA hydrogels was more than that in the Blank groups. $p_{3\&4}$SIS-CA/Exs hydrogels were more effective in promoting cell proliferation than SIS-CA/Exs hydrogels. Nevertheless, there was no statistical difference between the $p_{1\&2}$SIS-CA/Exs and $p_{3\&4}$SIS-CA/Exs hydrogels.

The cell adhesion behavior differences of different surfaces were investigated by cell images at time intervals of 12 and 24 h (Fig. 5e). From the morphology of the cells cultured for 12 h, SIS-CA/Exs hydrogels could significantly promote cell growth. Cells on SIS-CA/Exs hydrogels had been spread, while they were still in a spherical state and with a disordered cytoskeleton on plastic plates. This demonstrate that SIS-CA hydrogels, as ECM materials, simulate the growth environment of cells in the body. Furthermore, the pseudopodia of cells extended along the 3D network of hydrogels after 24 h of culturing. Spindle shape cells with clear lines of actin filaments (red color, Rhodamine phalloidin-labeled) could clearly be seen in $p_{3\&4}$SIS-CA/Exs hydrogels, and the density of cells increased. These results indicate that $p_{3\&4}$SIS-CA/Exs hydrogels are favorable scaffolds to permit growth and expansion of BMSCs.

3.5. SIS-CA/Exs hydrogels with fusion peptides promoting the differentiation of BMSCs

Designing scaffolds with osteogenic microenvironment that can induce osteogenic differentiation of BMSCs is of great significance to bone regenerative medicine. In order to evaluate whether BMSCs can be induced to differentiate toward osteoblastic lineages, the expression of osteogenesis-related genes (*Runx2*, *Alp* and *Opn*), as well as corresponding protein expression were assessed after 14 d of incubation in the osteogenic differentiation medium or basal medium. Among them, *Runx2* is the main transcription factor that initiates osteogenic differentiation [55], whereas *Alp* and *Opn* may contribute to the capture of calcium in bones and the growth of hydroxyapatite [56,57]. Real-time quantitative polymerase chain reaction (qRT-PCR) (Fig. 6a and Fig. S4a) data shows that the expression of *Runx2*, *Alp* and *Opn* significantly increased in hydrogels with BMSC-Exs compared with those in Blank groups and SIS-CA hydrogels. It is suggested that the differential expression of miRNA in exosomes such as miRNA-151–5p upregulate and miR-4532 downregulate, triggered the phosphatidylinositol 3-kinases/-serine/three-onlinekinase (PI3K/AKT) signaling pathway [26,58–60], thereby promoting the osteogenic differentiation of cells. Under osteogenic induction conditions, the expression level of *Runx2*, *Alp* and *Opn* in $p_{3\&4}$SIS-CA/Exs was higher than that of SIS-CA/Exs and $p_{1\&2}$SIS-CA/Exs. However, there was no significant difference in the expression level of *Opn* in $_{3\&4}$SIS-CA/Exs and $p_{1\&2}$SIS-CA/Exs in the basal medium. Overall, the fusion peptides with EAAAK have a positive effect on exosomes in promoting osteogenic differentiation of cells in vitro. To further corroborate the results from the qRT-PCR analysis, the expression of osteogenesis-related proteins was also probed. The quantified results (Fig. 6b and c) from western blot bands shows similar trends as qRT-PCR results. Fig. 6d and Fig. S4b visually shows the expression levels of relative proteins RUNX2, ALP and OPN in BMSCs. Among the three sets of fluorescence images, the cells of $p_{3\&4}$SIS-CA/Exs hydrogels emitted the strongest red fluorescence. The above results prove that fusion peptides are able to prolong the action time of exosomes. $p_{3\&4}$SIS-CA/Exs hydrogels significantly promote the osteogenic potential of the BMSCs.

3.6. SIS-CA/Exs hydrogels with fusion peptides promoting the bone regeneration in vivo

We prepared critical skull defects in rats with a diameter of 8 mm, which clearly reflects the role of hydrogels in bone regeneration, as the body cannot heal itself [61]. The regeneration effect of SIS-CA, SIS--CA/Exs, $p_{1\&2}$SIS-CA/Exs and $p_{3\&4}$SIS-CA/Exs hydrogels on skull bone defect are shown in Fig. 7a, Blank as control.12 weeks after surgery, restored connective tissue were filled in the whole defect areas in control groups, whereas other groups were more or less covered with bone-like tissue. The osteogenesis was further analyzed by micro-CT. The image shows that new bones were formed from edges to centers of the defect areas in all hydrogel groups. Notably, although some bone fragments were found in SIS-CA and SIS-CA/Exs hydrogel groups, the boundary between skull defects and surrounding host bone was still clearly visible, indicating the defect sites were still undergoing bone remodeling. The defects of $p_{1\&2}$SIS-CA/Exs and $p_{3\&4}$SIS-CA/Exs hydrogel groups were almost completely covered by regenerated bone. In particular, the surface morphology of healed defects closely resembled surrounding normal bone. The quantitative analyses of the bone volume fraction (BV/TV × 100%) of defect areas are shown in Fig. 7b. Compared with the lower values in control, SIS-CA and SIS-CA/Exs groups, BV fractions of calvarium in $p_{1\&2}$SIS-CA/Exs and $p_{3\&4}$SIS-CA/Exs groups were obviously increased. The values were not statistically different between $p_{1\&2}$SIS-CA/Exs and $p_{3\&4}$SIS-CA/Exs groups. The representative micro-CT images and quantitative data suggested that SIS-CA/Exs hydrogels with fusion peptides effectively activated bone repair process.

Hematoxylin and eosin (HE) staining, Masson's staining and immunohistochemical (IHC) staining provided more complementary details of the regenerated bone tissues. HE staining results (Fig. 8a) show no obvious inflammatory tissues in each group. In the control group, the defect area filled with fibrous tissue. Calcified bone tissue was observed in the SIS-CA groups. In $p_{1\&2}$SIS-CA/Exs and $p_{3\&4}$SIS-CA/Exs groups, newly formed bone was evenly distributed. The $p_{3\&4}$SIS-CA/Exs groups showed the best structural integrity in all groups. Masson's staining (Fig. 8b) was used to identity the collagen in bone matrix to observe the activity of osteogenesis [62]. The blue staining area (collagen) was larger in $p_{1\&2}$SIS-CA/Exs and $p_{3\&4}$SIS-CA/Exs groups than that in SIS-CA and SIS-CA/Exs groups, indicating that there is a lot of new bone.

IHC staining revealed osteogenic progression of all hydrogel groups for 12 weeks. RUNX2 positive area was described in Fig. 8c. In detail, the graphics revealed that SIS-CA hydrogels with BMSCs-Exs formed more new bone than control and SIS-CA groups. Obvious RUNX2 staining was detected in $p_{1\&2}$SIS-CA/Exs and $p_{3\&4}$SIS-CA/Exs groups than other groups. The highest expression level in $p_{3\&4}$SIS-CA/Exs groups suggested that $p_{3\&4}$SIS-CA/Exs hydrogels had the strongest effect on bone regeneration. Briefly, in the defect models treated with $p_{3\&4}$SIS-CA/Exs hydrogels, regenerated bone tissue formed in the hollow area of the defect model due to a large number of exosomes were captured by fusion peptides. In this case, hydrogels filled in the defect space not only provided mechanical support, but also prolonged the action time of the exosomes as the degradation of the hydrogels and fusion peptides occurred. Consequently, the mechanical strength and biomimetic microenvironment of $p_{3\&4}$SIS-CA/Exs hydrogels lead to the great effect of bone regeneration.

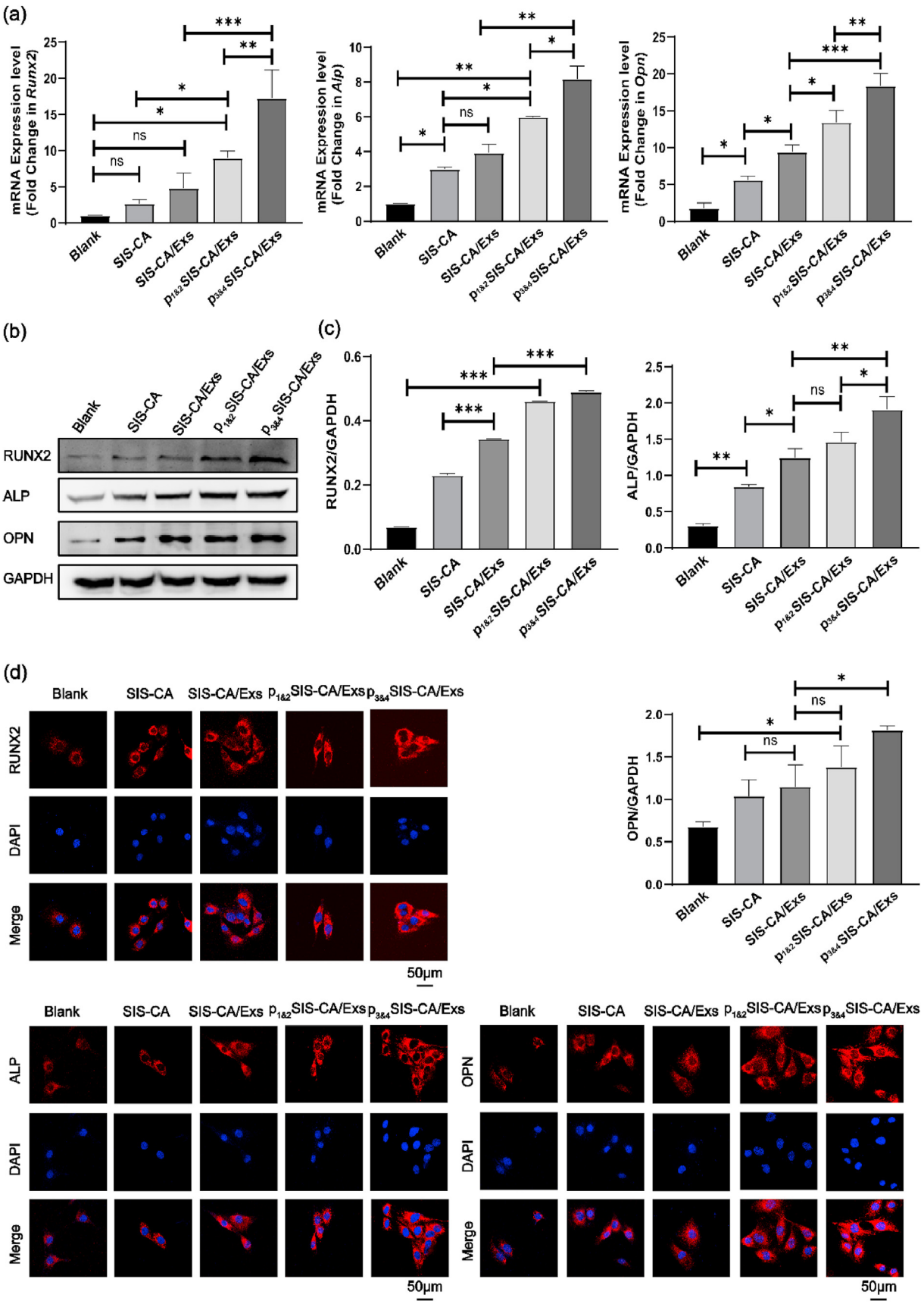

Fig. 6. Osteogenic differentiation of BMSCs. (a) The expression levels of osteogenesis-related genes *Runx2*, *Alp* and *Opn* on the 14th d osteogenic induction, normalizing to GAPDH (n = 3). (b) The expression levels of osteogenesis-related proteins RUNX2, ALP and OPN on the 14th d osteogenic induction, normalizing to GAPDH. (c) Quantitative expression of osteogenesis-related proteins on the 14th d of osteogenic induction (n = 3). (d) Immunofluorescence analysis of osteogenesis-related proteins RUNX2, ALP and OPN expressed in BMSCs. DAPI(Blue) labeled nucleus. *$p < 0.05$, **$p < 0.01$ and ***$p < 0.001$.

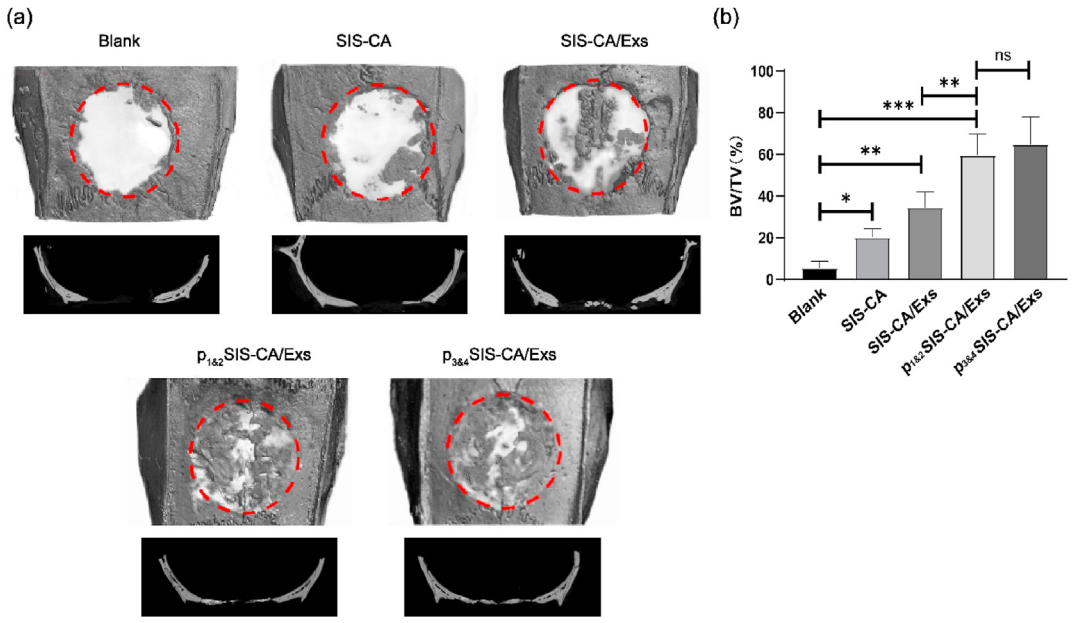

Fig. 7. Micro-CT images of new bone formation in the defect at 12 weeks after injection of SIS-CA, SIS-CA/Exs, $p_{1\&2}$SIS-CA/Exs, $p_{3\&4}$SIS-CA/Exs hydrogels, Blank as control. (a) 3D reconstruction and sagittal images of bone defects. (b) Quantitative analysis of BV/TV of the skull defects (n = 6). *p < 0.05, **p < 0.01 and ***p < 0.001.

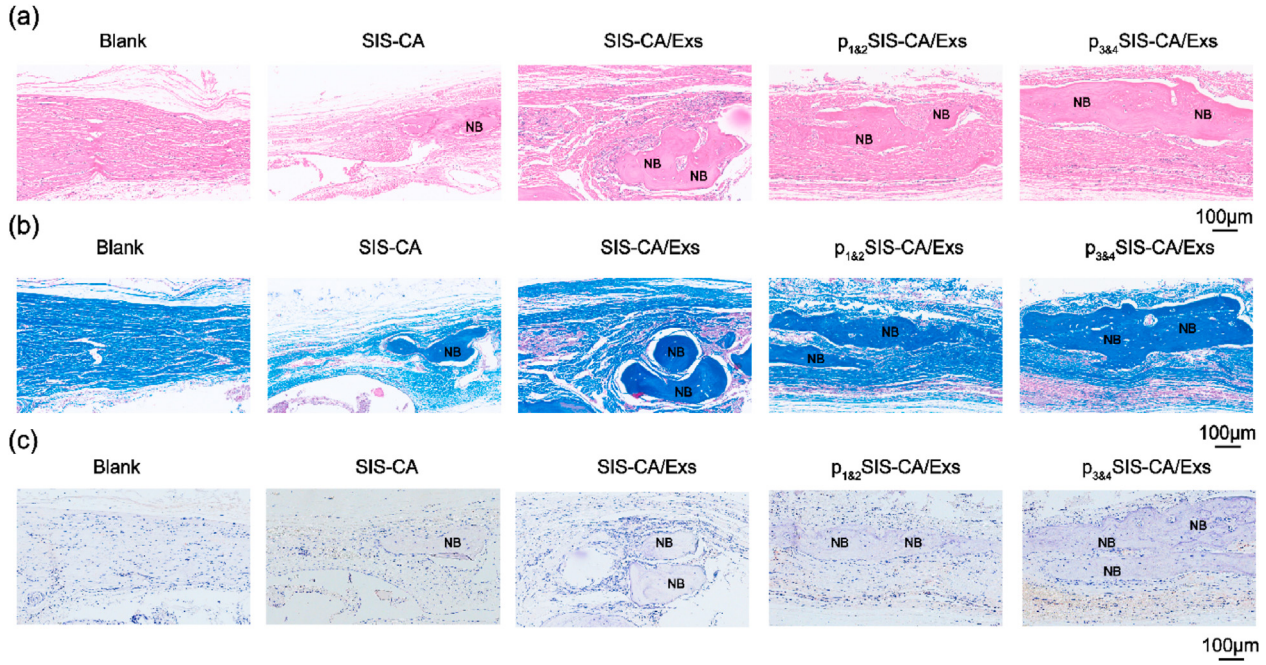

Fig. 8. Histological evaluations and IHC staining for bone regeneration. Representative (a) H&E and (b) Masson's staining histological images of bone regeneration at 12 weeks post-surgery, Blank as control. (c) IHC staining of skull defect sections for RUNX2 expression at 12 weeks post-implantation. The brown color represents positive staining. NB: new bone.

4. Conclusion

In summary, excellent injectable thermo-sensitive $p_{3\&4}$SIS-CA/Exs hydrogels were developed. The incorporation of CA significantly improved the mechanical properties of hydrogels and supported hydrogels to maintain shape for a long time. BMSCs-Exs provided a bionic microenvironment to enhance the proliferation and osteogenic differentiation of BMSCs, showing superior performance for bone repair. Moreover, BMSC-Exs were successfully introduced into hydrogels through fusion peptides. The fusion peptides containing EAAAK exhibited stronger biological activity, promoted the positive effect of exosomes on osteogenic differentiation of BMSCs. The preparation method of the material is simple and economical, while it has the advantages of reducing the risk of immunogenic reaction and superior stability. It is expected to become a promising material in bone regenerative medicine. Apprises objectively, future research needs to clarify the proportion of each component in hydrogels, further optimize the mechanical properties and osteogenic ability of hydrogels. In addition, a variety of bone defect models should be constructed for research, in order to realize the transition from basic research to clinical application.

Credit author statement

Shiqing Ma: Conceptualization, Investigation, Data curation, Methodology, Writing – original draft. Jinzhe Wu: Investigation, Data curation, Methodology, Writing – original draft. Han Hu: Investigation, Data collection, Software. Yuzhu Mu: Data collection, Formal analysis and interpretation. Lei Zhang: Data analysis and interpretation, Visualization. Yifan Zhao: Visualization. Xiaowei Bian: Visualization. Wei Jing: Critical revision of the article. Pengfei Wei: Conceptualization, Supervision. Bo Zhao: Resources, Project administration. Jiayin Deng: Resources, Project administration. Zihao liu: Resources, Project administration, Final approval of the version to be published.

Declaration of competing interest

The authors declare that they have no known competing financial interests or personal relationships that could have appeared to influence the work reported in this paper.

Acknowledgements

S.M. and J.W. contributed equally to this work. This work was supported by the National Natural Science Foundation of China (NSFC, Grant No. 81701019), the China Postdoctoral Science Foundation (Grant Nos. 2020M680253), the Scientific Foundation of Tianjin Education Commission (Grant No. 2019KJ173), and the Science and technology project of Tianjin Health Committee (Grant No. QN20026). Scientific research foundation of Stomatological Hospital of Tianjin Medical University (Grant No. 2020YKY06). Guangdong Basic and Applied Basic Research Foundation (Grant No. 2020A1515111182).

Appendix A. Supplementary data

Supplementary data to this article can be found online at https://doi.org/10.1016/j.mtbio.2021.100195.

References

[1] A.M. Pobloth, S. Checa, H. Razi, A. Petersen, J.C. Weaver, K. Schmidt-Bleek, M. Windolf, A. Tatai, C.P. Roth, K.D. Schaser, Mechanobiologically optimized 3D titanium-mesh scaffolds enhance bone regeneration in critical segmental defects in sheep, Sci. Transl. Med. 10 (2018), eaam8828, https://doi.org/10.1126/scitranslmed.aam8828.

[2] K. Zhou, P. Yu, X. Shi, T. Ling, Z. Zhou, Hierarchically porous hydroxyapatite hybrid scaffold incorporated with reduced graphene oxide for rapid bone ingrowth and repair, ACS Nano 13 (2019) 9595–9606, https://doi.org/10.1021/acsnano.9b04723.

[3] W. Shi, M. Sun, X. Hu, B. Ren, J. Cheng, C. Li, X. Duan, X. Fu, J. Zhang, H. Chen, Structurally and functionally optimized silk-fibroin-gelatin scaffold using 3D printing to repair cartilage injury in vitro and in vivo, Adv. Mater. 29 (2017), 1701089.1, https://doi.org/10.1002/adma.201701089.

[4] P. Jayaraman, C. Gandhimathi, J.R. Venugopal, D.L. Becker, S. Ramakrishna, D.K. Srinivasan, Controlled release of drugs in electrosprayed nanoparticles for bone tissue engineering, Adv. Drug Deliv. Rev. 94 (2015) 77–95, https://doi.org/10.1016/j.addr.2015.09.007.

[5] K. Healy, Temperature-sensitive hydrogels in tissue engineering, Faseb. J. 4 (2006) A21, https://doi.org/10.1096/fasebj.20.4.A21-b.

[6] Y. Li, J. Cao, S. Han, Y. Liang, T. Zhang, H. Zhao, L. Wang, Y. Sun, ECM based injectable thermo-sensitive hydrogel on the recovery of injured cartilage induced by osteoarthritis, Artif. Cells Nanomed. Biotechnol. 46 (2018) 152–160, https://doi.org/10.1080/21691401.2018.1452752.

[7] K. Narendra, Doo Singh, Lee Sung, In situ gelling pH- and temperature-sensitive biodegradable block copolymer hydrogels for drug delivery, J. Contr. Release 193 (2014) 214–227, https://doi.org/10.1016/j.jconrel.2008.01.005.

[8] H.K. Kim, W.S. Shim, S.E. Kim, K.H. Lee, D.S. Lee, Injectable in situ-forming pH/thermo-sensitive hydrogel for bone tissue engineering, Tissue Eng. 15 (2009) 923–933, https://doi.org/10.1089/ten.tea.2007.0407.

[9] K. Kim, M.S. Kim, An injectable hydrogel derived from small intestine submucosa as a stem cell carrier, J. Biomed. Mater. Res. B Appl. Biomater. 104 (2016) 1544–1550, https://doi.org/10.1002/jbm.b.33504.

[10] W. Wang, X. Zhang, N.-N. Chao, T.-W. Qin, W. Ding, Y. Zhang, J.-W. Sang, J.-C. Luo, Preparation and characterization of pro-angiogenic gel derived from small intestinal submucosa, Acta Biomater. 29 (2016) 135–148, https://doi.org/10.1016/j.actbio.2015.10.013.

[11] J.W. Choi, J.K. Park, J.W. Chang, D.Y. Kim, C.H. Kim, Small intestine submucosa and mesenchymal stem cells composite gel for scarless vocal fold regeneration, Biomaterials 35 (2014) 4911–4918, https://doi.org/10.1016/j.biomaterials.2014.03.008.

[12] M.T. Spang, K.L. Christman, Extracellular matrix hydrogel therapies: in vivo applications and development, Acta Biomater. 68 (2017) 1–14, https://doi.org/10.1016/j.actbio.2017.12.019.

[13] R. Xing, L. Kai, T. Jiao, Z. Ning, X. Yan, An injectable self-assembling collagen-gold hybrid hydrogel for combinatorial antitumor photothermal/photodynamic therapy, Adv. Mater. 28 (2016) 3669–3676, https://doi.org/10.1002/adma.201600284.

[14] G.G. Giobbe, C. Crowley, C. Luni, S. Campinoti, M. Khedr, K. Kai, M. Santis, E. Zambaiti, F. Michielin, L. Meran, Extracellular matrix hydrogel derived from decellularized tissues enables endodermal organoid culture, Nat. Commun. 10 (2019) 5658, https://doi.org/10.1038/s41467-019-13605-4.

[15] Z. Farhan, R.B. Hinton, R.A. Moore, B.R. Scott, B. Roosevelt, D.A. Narmoneva, M. Taylor, D.L. Morales, Physiological growth, remodeling potential, and preserved function of a novel bioprosthetic tricuspid valve: tubular bioprosthesis made of small intestinal submucosa-derived extracellular matrix, J. Am. Coll. Cardiol. 66 (2015) 877–888, https://doi.org/10.1016/j.jacc.2015.06.1091.

[16] C. Luo, H. Fang, M. Zhou, J. Li, Z. Wang, Biomimetic open porous structured core-shell microtissue with enhanced mechanical properties for bottom-up bone tissue engineering, Theranostics 9 (2019) 4663–4677, https://doi.org/10.7150/thno.34464.

[17] C. Chen, D. Li, H. Yano, K. Abe, Insect cuticle-mimetic hydrogels with high mechanical properties achieved via the combination of chitin nanofiber and gelatin, J. Agric. Food Chem. 67 (2019) 5571–5578, https://doi.org/10.1021/acs.jafc.9b00984.

[18] D. Wang, J. Zhang, Y. Zhong, M. Chu, W. Chang, Z. Yao, Mussel-inspired biocompatible free-standing adhesive films assembled layer-by-layer with water-resistance, RSC Adv. 8 (2018) 18904–18912, https://doi.org/10.1039/C8RA03214A.

[19] L. Duan, Q. Yuan, H. Xiang, X. Yang, L. Liu, J. Li, Fabrication and characterization of a novel collagen-catechol hydrogel, J. Biomater. Appl. 32 (2017) 862–870, https://doi.org/10.1177/0885328217747125.

[20] S. Lin, G. Yang, F. Jiang, M. Zhou, X. Jiang, A magnesium-enriched 3D culture system that mimics the bone development microenvironment for vascularized bone regeneration, Adv. Sci. 6 (2019), 1900209, https://doi.org/10.1002/advs.201900209.

[21] D. Gonzalez-Nieto, L. Li, A. Kohler, G. Ghiaur, E. Ishikawa, A. Sengupta, M. Madhu, J.L. Arnett, R.A. Santho, S.K. Dunn, Connexin-43 in the osteogenic BM niche regulates its cellular composition and the bidirectional traffic of hematopoietic stem cells and progenitors, Blood 119 (2012) 5144–5154, https://doi.org/10.1182/blood-2011-07-368506.

[22] L. Lidgren, I.Q. Arun, K. Teotia, Prerna Singh, Ankita Mishra, Deepika Jaiman, Jukka Seppala, Lars Lidgren, Ashok Kumar, Exosome-functionalized ceramic bone substitute promotes critical-sized bone defect repair in rats, ACS Appl. Bio. Mater. (2021). https://pubs.acs.org/doi/pdf/10.1021/acsabm.1c00311.

[23] J.L. Crane, C. Xu, Bone marrow mesenchymal stem cells and TGF-β signaling in bone remodeling, J. Clin. Invest. 124 (2014) 466–472, https://doi.org/10.1172/JCI70050.

[24] Zhang Xiaoqing, P. Michelle, Craig A. Bendeck, J. Paul Simmons, Deriving vascular smooth muscle cells from mesenchymal stromal cells: evolving differentiation strategies and current understanding of their mechanisms, Biomaterials 145 (2017) 9–22, https://doi.org/10.1016/j.biomaterials.2017.08.028.

[25] S.R. Baglio, D.M. Pegtel, N. Baldini, Mesenchymal stem cell secreted vesicles provide novel opportunities in (stem) cell-free therapy, Front. Physiol. 3 (2012) 359, https://doi.org/10.3389/fphys.2012.00359.

[26] T. Furuta, S. Miyaki, H. Ishitobi, T. Ogura, Y. Kato, N. Kamei, K. Miyado, Y. Higashi, M. Ochi, Mesenchymal stem cell-derived exosomes promote fracture healing in a mouse model, Stem Cells Transl. Med. 5 (2016) 1620–1630, https://doi.org/10.5966/sctm.2015-0285.

[27] X. Liu, Y. Yang, Y. Li, X. Niu, B. Zhao, Y. Wang, C. Bao, Z. Xie, Q. Lin, L. Zhu, Integration of stem cell-derived exosomes with in situ hydrogel glue as a promising tissue patch for articular cartilage regeneration, Nanoscale 9 (2017) 4430–4438, https://doi.org/10.1039/c7nr00352h.

[28] L. Mei, X. Zhao, H. Xing, Z. Xu, N.S. Zhu, L. Lang, T. Yang, C. Cai, D. Wang, P. Ding, Comparison of exosome-mimicking liposomes with conventional liposomes for intracellular delivery of siRNA, Int. J. Pharm. 550 (2018) 100–113, https://doi.org/10.1016/j.ijpharm.2018.08.040.

[29] Y. Yang, Y. Ye, X. Su, J. He, W. Bai, X. He, MSCs-derived exosomes and neuroinflammation, neurogenesis and therapy of traumatic brain injury, Front. Cell. Neurosci. 11 (2017) 55, https://doi.org/10.3389/fncel.2017.00055.

[30] G. Ran, W. Fang, L. Zhang, Y. Peng, Y. He, Polypeptides IGF-1C and P24 Synergistically Promote Osteogenic Differentiation of Bone Marrow Mesenchymal Stem Cells in Vitro through the P38 and JNK Signaling Pathways, 2021, https://doi.org/10.1101/2021.06.09.447738.

[31] R. Xu, S. Xiang, Y. Si, F. Yu, W. Zhu, T. Xiao, Z. Fu, Z. Ping, C. Jie, H. Jiang, MicroRNA-31a-5p from aging BMSCs links bone formation and resorption in the aged bone marrow microenvironment, Aging Cell 17 (2018), e12794, https://doi.org/10.1111/acel.12794.

[32] A. Pape, M.H. Bakker, C. Tseng, M. Bastings, S. Koudstaal, P. Agostoni, S. Chamuleau, P. Dankers, An injectable and drug-loaded supramolecular hydrogel for local catheter injection into the pig heart, JoVE 100 (2015), e52450, https://doi.org/10.3791/52450.

[33] C. Han, J. Zhou, C. Liang, B. Liu, X. Pan, Y. Zhang, Y. Wang, B. Yan, W. Xie, F. Liu, Human umbilical cord mesenchymal stem cell derived exosomes encapsulated in

functional peptide hydrogels promote cardiac repair, Biomater. Sci. 7 (2019) 2920–2933, https://doi.org/10.1039/c9bm00101h.
[34] J. Wang, W. Li, L. Zhang, L. Ban, P. Chen, W. Du, X. Feng, B.F. Liu, Chemically edited exosomes with dual ligand purified by microfluidic device for active targeted drug delivery to tumor cells, ACS Appl. Mater. Interfaces 9 (2017) 27441–27452, https://doi.org/10.1021/acsami.7b06464.
[35] J. Yang, Y. Shimada, R.C.L. Olsthoorn, B.E. Snaar-Jagalska, H.P. Spaink, A. Kros, Application of coiled coil peptides in liposomal anticancer drug delivery using a zebrafish xenograft model, ACS Nano 10 (2016) 7428–7435, https://doi.org/10.1021/acsnano.6b01410.
[36] X. Gao, N. Ran, X. Dong, B. Zuo, R. Yang, Q. Zhou, H.M. Moulton, Y. Seow, H. Yin, Anchor peptide captures, targets, and loads exosomes of diverse origins for diagnostics and therapy, Sci. Transl. Med. 10 (2018), eaat0195, https://doi.org/10.1126/scitranslmed.aat0195.
[37] Yousefpour Parisa, Jonathan McDaniel, Varun Prasad Lucie, Xinghai Ahn, Genetically encoding albumin binding into chemotherapeutic-loaded polypeptide nanoparticles enhances their antitumor efficacy, Nano Lett. 18 (2018) 7784–7793, https://doi.org/10.1021/acs.nanolett.8b03558.
[38] N. Yim, S.W. Ryu, K. Choi, K.R. Lee, S. Lee, H. Choi, J. Kim, M.R. Shaker, W. Sun, J.H. Park, Exosome engineering for efficient intracellular delivery of soluble proteins using optically reversible protein-protein interaction module, Nat. Commun. 7 (2016) 12277, https://doi.org/10.1038/ncomms12277.
[39] J.M. Vicencio, D.M. Yellon, V. Sivaraman, D. Das, C. Boi-Doku, Plasma exosomes protect the myocardium from ischemia-reperfusion injury, J. Am. Coll. Cardiol. 65 (2015) 1525–1536, https://doi.org/10.1016/j.jacc.2015.02.026.
[40] T.M. Chiang, F. Cole, V. Woo-Rasberry, Cloning, characterization, and functional studies of a 47-kDa platelet receptor for type III collagen, J. Biol. Chem. 277 (2002) 34896–34901, https://doi.org/10.1074/jbc.M205311200.
[41] X. Xu, W. Yao, J.L. Lauer-Fields, G.B. Fields, B. Steffensen, Contributions of the MMP-2 collagen binding domain to gelatin cleavage. Substrate binding via the collagen binding domain is required for hydrolysis of gelatin but not short peptides, Matrix Biol. 23 (2005) 171–181, https://doi.org/10.1016/j.matbio.2004.05.002.
[42] J. Mcmasters, A. Panitch, Collagen-binding nanoparticles for extracellular anti-inflammatory peptide delivery decrease platelet activation, promote endothelial migration, and suppress inflammation, Acta Biomater. 49 (2016) 78–88, https://doi.org/10.1016/j.actbio.2016.11.023.
[43] J. Dai, Vascularization and cellularization of collagen scaffolds incorporated with two different collagen-targeting human basic fibroblast growth factors, J. Biomed. Mater. Res. A. 82 (2010) 630–636, https://doi.org/10.1002/jbm.a.31179.
[44] Z. Liu, S. Ma, S. Duan, D. Xuliang, Y. Sun, X. Zhang, X. Xu, B. Guan, C. Wang, M. Hu, X. Qi, X. Zhang, P. Gao, Modification of titanium substrates with chimeric peptides comprising antimicrobial and titanium-binding motifs connected by linkers to inhibit biofilm formation, ACS Appl. Mater. Interfaces 8 (2016) 5124–5136, https://doi.org/10.1021/acsami.5b11949.
[45] X. Chen, J.L. Zaro, W.-C. Shen, Fusion protein linkers: property, design and functionality, Adv. Drug Deliv. Rev. 65 (2013) 1357–1369, https://doi.org/10.1016/j.addr.2012.09.039.
[46] L.Z. Hong, Q.Y. Xue, X. Chong, W. Yang, H.X. Xiang, M.L. Zhi, Increasing the homogeneity, stability and activity of human serum albumin and interferon-alpha2b fusion protein by linker engineering, Protein Expr. Purif. 61 (2008) 73–77, https://doi.org/10.1016/j.pep.2008.04.013.
[47] M. Lee, K. Bang, H. Kwon, S. Cho, Enhanced antibacterial activity of an attacin-coleoptericin hybrid protein fused with a helical linker, Mol. Biol. Rep. 40 (2013) 3593–3960, https://doi.org/10.1007/s11033-012-2472-4.
[48] V. Kahn, V. Zakin, Effect of salicylhydroxamic acid (sham) on dl-dopa oxidation by mushroom tyrosinase and by $NaIO_4$, J. Food Biochem. 24 (2000) 399–415, https://doi.org/10.1111/j.1745-4514.2000.tb00709.x.
[49] J. Zhao, Y.F. Yan, Y.Z. Shang, Y. Du, L.X. Long, X. Yuan, X. Hou, Thermosensitive elastin-derived polypeptide hydrogels crosslinked by genipin, Int. J. Polym. Mater. (2016), https://doi.org/10.1080/00914037.2016.1217534.
[50] J. Lopes, M. Correia, I. Martins, A.G. Henriques, I. Delgadillo, C. Da, A. Nunes, FTIR and Raman spectroscopy applied to dementia diagnosis through analysis of biological fluids, J. Alzheimers. Dis. 52 (2016) 801–812, https://doi.org/10.3233/JAD-151163.
[51] A. Sionkowska, Thermal and mechanical properties of UV irradiated collagen/chitosan thin films, Polym. Degrad. Stabil. 91 (2009) 3026–3032, https://doi.org/10.1016/j.polymdegradstab.2006.08.009.
[52] C. Théry, L. Zitvogel, S. Amigorena, Exosomes: composition, biogenesis and function, Nat. Rev. Immunol. 2 (2002) 569–579, https://doi.org/10.1038/nri855.
[53] G. Raposo, W. Stoorvogel, Extracellular vesicles: exosomes, microvesicles, and friends, J. Cell Biol. 200 (2013) 373–383, https://doi.org/10.1083/jcb.201211138.
[54] W. Li, Y. Liu, P. Zhang, Y. Tang, M. Zhou, W. Jiang, X. Zhang, G. Wu, Y. Zhou, Tissue-engineered bone immobilized with human adipose stem cells-derived exosomes promotes bone regeneration, ACS Appl. Mater. Interfaces 10 (2018) 5240–5254, https://doi.org/10.1021/acsami.7b17620.
[55] L. Li, J. Li, J. Guo, H. Zhang, X. Zhang, C. Yin, L. Wang, Y. Zhu, Q. Yao, Biomimetic scaffolds: 3D molecularly functionalized cell-free biomimetic scaffolds for osteochondral regeneration, Adv. Funct. Mater. 29 (2019), 1807356, https://doi.org/10.1002/adfm.201970036, 1.
[56] J.P. Schroeppel, J.D. Crist, H.C. Anderson, J. Wang, Molecular regulation of articular chondrocyte function and its significance in osteoarthritis, Histol. Histopathol. 26 (2011) 377–394, https://doi.org/10.14670/HH-26.377.
[57] F. Liu, L. Malaval, Global amplification polymerase chain reaction reveals novel transitional stages during osteoprogenitor differentiation, J. E. Aubin, J. Cell. Sci. 116 (2003) 1787–1796, https://doi.org/10.1242/jcs.00376.
[58] R. Xu, S. Xiang, Y. Si, F. Yu, W. Zhu, T. Xiao, Z. Fu, Z. Ping, C. Jie, H. Jiang, MicroRNA-31a-5p from aging BMSCs links bone formation and resorption in the aged bone marrow microenvironment, Aging Cell 17 (2018), e12794, https://doi.org/10.1111/acel.12794.
[59] Y. Qin, L. Wang, Z. Gao, G. Chen, C. Zhang, Bone marrow stromal/stem cell-derived extracellular vesicles regulate osteoblast activity and differentiation in vitro and promote bone regeneration in vivo, Sci. Rep. 6 (2016) 21961, https://doi.org/10.1038/srep21961.
[60] X. Wang, O. Omar, V. Forugh, T. Peter, E. Karin, X.M. Shi, Mesenchymal stem cell-derived exosomes have altered microRNA profiles and induce osteogenic differentiation depending on the stage of differentiation, PLoS One 13 (2018), e0193059, https://doi.org/10.1371/journal.pone.0193059.
[61] J.O. Hollinger, J.C. Kleinschmidt, The critical size defect as an experimental model to test bone repair materials, J. Craniofac. Surg. 1 (1989) 60–68, https://doi.org/10.1097/00001665-199001000-00011.
[62] Y. Mu, S. Ma, P. Wei, Y. Wang, W. Jing, Y. Zhao, L. Zhang, J. Wu, B. Zhao, J. Deng, Z. Liu, Multifunctional modification of SIS membrane with chimeric peptides to promote its antibacterial, osteogenic, and healing-promoting abilities for applying to GBR, Adv. Funct. Mater. (2021), 2101452, https://doi.org/10.1002/adfm.202101452.